

Article

Exploring Dielectric and Magnetic Properties of Ni and Co Ferrites through Biopolymer Composite Films

Júlio C. Góes ¹, Sónia D. Figueiró ¹, Karlo David A. Sabóia ¹, Yana Luck Nunes ², António César H. Barreto ², Pierre Basílio Almeida Fechine ² , Susana Devesa ³ , António Sérgio Bezerra Sombra ¹, Manuel A. Valente ⁴ , Sílvia Rodrigues Gavinho ⁴  and Manuel Pedro Fernandes Graça ^{4,*} 

- ¹ Laboratório de Telecomunicações e Ciência e Engenharia dos Materiais (LOCEM), Departamento de Física, Universidade Federal do Ceará, Fortaleza 1315, Brazil; jcgoes@fisica.ufc.br (J.C.G.); soniafigueiro@fisica.ufc.br (S.D.F.); k.d.saboia@gmail.com (K.D.A.S.); sombra@fisica.ufc.br (A.S.B.S.)
- ² Grupo de Química de Materiais Avançados (CGMAT), Departamento de Química Analítica e Físico-Química, Universidade Federal do Ceará, Fortaleza 1315, Brazil; yal Luck@hotmai.com (Y.L.N.); antoniocesarhb@hotmail.com (A.C.H.B.); fechine@ufc.br (P.B.A.F.)
- ³ Centre for Mechanical Engineering, Materials and Processes (CEMMPRE), Advanced Production and Intelligent Systems (ARISE), Department of Mechanical Engineering, University of Coimbra, Rua Luís Reis Santos, 3030-788 Coimbra, Portugal; sdevesa@dem.uc.pt
- ⁴ I3N-Physics Department, University of Aveiro, Campus Santiago, 3810-193 Aveiro, Portugal; mav@ua.pt (M.A.V.); silviagavinho@ua.pt (S.R.G.)
- * Correspondence: mpfg@ua.pt

Abstract: This study explores the synthesis and characterization of chitosan/gelatine films incorporating nickel ferrite (NiFe₂O₄) and cobalt ferrite (CoFe₂O₄) nanoparticles. The magnetic nanoparticles exhibit superparamagnetic behaviour, making them attractive for various applications, including biomedical uses. The X-ray diffraction analysis confirmed the successful synthesis of NiFe₂O₄ and CoFe₂O₄ nanoparticles, and the scanning electron micrographs illustrated well-dispersed ferrite nanoparticles within the biopolymer network, despite the formation of some aggregates attributed to magnetic interactions. Magnetization loops revealed lower saturation magnetization values for the composites, attributed to the chitosan/gelatine coating and the dielectric studies, indicating increased dielectric losses in the presence of ferrites, particularly pronounced in the case of NiFe₂O₄, suggesting interactions at the interface region between the polymer and ferrite particles. The AC conductivity shows almost linear frequency dependence, associated with proton polarization and conduction processes, more significant at higher temperatures for samples with ferrite particles.

Keywords: biocomposite; magnetic nanoparticles; nickel ferrite; cobalt ferrite; chitosan; gelatine



Citation: Góes, J.C.; Figueiró, S.D.; Sabóia, K.D.A.; Nunes, Y.L.; Barreto, A.C.H.; Fechine, P.B.A.; Devesa, S.; Sombra, A.S.B.; Valente, M.A.; Gavinho, S.R.; et al. Exploring Dielectric and Magnetic Properties of Ni and Co Ferrites through Biopolymer Composite Films. *Magnetochemistry* **2024**, *10*, 20. <https://doi.org/10.3390/magnetochemistry10040020>

Received: 29 February 2024
Revised: 25 March 2024
Accepted: 28 March 2024
Published: 29 March 2024



Copyright: © 2024 by the authors. Licensee MDPI, Basel, Switzerland. This article is an open access article distributed under the terms and conditions of the Creative Commons Attribution (CC BY) license (<https://creativecommons.org/licenses/by/4.0/>).

1. Introduction

Magnetic nanoparticles (MNs) are currently under extensive investigation in both liquid organic media and polymer matrices [1–3]. MNs have attracted researchers in various fields such as physics, medicine, biology and materials science due to their multifunctional properties such as small size, superparamagnetic, low toxicity, etc. [4–8].

Among different magnetic nanomaterials, magnetite, Fe₃O₄, and maghemite, Fe₂O₃, have been extensively studied for biomedical applications due to their unique properties. However, a challenge to be addressed regarding iron oxide nanoparticles is their poor magnetic properties at small sizes and under physiological conditions. Moreover, the presence of iron atoms in these nanoparticles results in interactions with haemoglobin, leading to adverse effects [9].

Spinel ferrites nanomaterials with the general chemical formula of MFe₂O₄, where M = Mn, Co, Ni, Zn or other transition metals, can display superparamagnetic properties below a certain nanoparticle size range. Due to this magnetic behaviour and their phase structure stability, such functional nanoparticles have been exploited for several potential

biomedical applications, such as contrast agents for magnetic resonant imaging, drug delivery systems and magnetic hyperthermia agents, but also as a promising material for the solid-phase extraction of noble metals from leaching solutions of waste electrical and electronic equipment [10]. Additionally, the diversity of the synthesis techniques and parameters makes ferrites popular materials [11,12].

These spinel ferrites crystalize into an FCC (Face-Centred Cubic) lattice, which is formed by the oxygen anions with the metal cations occupying the octahedral and tetrahedral interstitial sites. Site occupancy is determined by the temperature, size of the cation and bonding preferences of the individual ions.

Considering A and B as the divalent and trivalent cations, this representation can be performed by the chemical formula $(A_{1-\chi}B_{\chi})[A_{\chi}B_{2-\chi}]O_4$, with the round and square parenthesis representing the tetrahedral and octahedral sites, respectively.

The degree of inversion, denoted as χ , quantifies the fraction of tetrahedral sites occupied by B cations. It ranges from 0, indicating a “normal” configuration, to 1, signifying an “inverse” structure for the spinel arrangement [13].

Among the spinel ferrite family, nickel ferrite, $NiFe_2O_4$, is one of the well-known inverse spinel soft magnetic materials, in which Fe^{3+} ions equally distribute both the tetrahedral and octahedral positions, whereas Ni^{2+} ions appear to occupy the octahedral site only [9], which can be represented as $(Fe)[NiFe]O_4$.

Usually, cobalt ferrite, $CoFe_2O_4$, also has an inverse spinel structure, in which Co^{2+} ions are in the octahedral positions and Fe^{3+} ions are equally distributed in the tetrahedral and octahedral sites. However, in nanostructured regimes, depending on the preparation techniques used, the inversion parameter varies and is found to exist in a mixed spinel structure [14,15].

Nickel ferrite has a net magnetic moment per molecule, high Curie temperature, high magnetization, high permeability, good electrical resistivity, and a low dielectric loss [9]. In turn, cobalt ferrite presents excellent physical properties such as high coercivity, medium saturation magnetization and large magneto-crystalline anisotropy, as well as excellent hardness and chemical stability [16].

However, MNs tend to aggregate due to strong magnetic dipole–dipole attractions between particles. So, stabilizers such as surfactants, oxides, metal nanoparticles or polymeric compounds, with some specific functional groups, have been used to modify these particles to increase their stability [17–19]. Magnetic particles usually consist of magnetic cores to ensure a strong magnetic response and a polymeric shell to provide favourable functional groups and features for diverse applications [20,21].

Natural polysaccharides and proteins, like chitosan (C) and gelatine (G), have been preferred to modify the magnetite nanoparticles because of excellent features such as hydrophilicity, biocompatibility, biodegradability and a remarkable affinity for metal ions [21–25]. These biopolymers are a well-known adsorbent and effective in the adsorption of metal ions since the amino ($-NH_2$), carboxyl ($-COOH$) and hydroxyl ($-OH$) groups on C–G chains can serve as electrostatic interaction and coordination sites [25–27].

Chitosan is a cationic polysaccharide obtained by the deacetylation of chitin, a natural polymer that can be found in the exoskeleton of crustaceans, insects and some fungi. Chitosan’s broad application in the medical and pharmaceutical fields is attributed to its inherent properties, such as biodegradability, biocompatibility, bioadsorbability, non-toxicity and easy chemical modification by the presence of functional groups ($-NH_2$, $-OH$) in its chemical structure that consists of N-acetyl-D-glucosamine and D-glucosamine units [28–31].

Gelatine is a protein obtained by partial hydrolysis of collagen, the main fibrous protein constituent in tissues, like bone, cartilage and skin. The amino acid composition of gelatine is based principally on glycine, proline and hydroxyproline. Due to its biological properties, gelatine has long been used in pharmaceutical and dietary supplements [32–34].

This study investigated thin films of natural polymers, chitosan and gelatine, containing nickel ferrite and cobalt ferrite nanoparticles, aiming to provide insights into the

structural and functional characteristics of the composite materials, evaluating the ability of ferrite particles and the chitosan/gelatine biopolymer blend to create a naturally occurring composite with magnetic properties and gather valuable information for future studies on potential applications in devices or in the field of environmental purification from oil pollution [31,35]. The investigation employed X-ray diffraction, scanning electron microscopy, dielectric spectroscopy and vibrating sample magnetometry.

2. Materials and Methods

2.1. Samples Preparation

The synthesis of NPs of Ni and Co ferrites was conducted by the co-precipitation processing route [36].

All reagents, the $\text{FeCl}_3 \cdot 6\text{H}_2\text{O}$, $\text{CoCl}_2 \cdot 6\text{H}_2\text{O}$, $\text{NiCl}_2 \cdot 6\text{H}_2\text{O}$ and NH_4OH solutions, are commercial products of analytical grade (purity > 99.9%), used without further purification, and supplied by Sigma-Aldrich and Vetec Química.

The solution of metallic salts containing $\text{M}^{2+}/\text{Fe}^{3+}$ (where M^{2+} denotes Co^{2+} or Ni^{2+}) was dissolved and mixed in milli-Q water in the ratio molar of 1:2 forming a spinel lattice phase (MFe_2O_4). The aqueous mixtures were heated at 80 °C and then added into a 30% wt. NH_4OH solution, under vigorous stirring, until pH 10 was reached, to form a black precipitate. The precipitate was washed several times with milli-Q water until the residual solution became neutral. Finally, the magnetic nanoparticles were dried in a desiccator and, after that, calcined at 400 °C for 1 h, in an air atmosphere, to form the spinel phases and improve their magnetic properties [36].

Chitosan, C, fully deacetylated (Sigma-Aldrich, St. Louis, MO, USA), was dissolved in an acetic acid solution (1% *v/v*) with mechanical stirring for 6 h. After centrifugation at 5000 rpm for 1 h, a dry matter was obtained after treatment in an oven, at 105 °C, until a constant weight corresponding to 20 mg/mL was reached. A solution of gelatine, G, (Vetec Química, Rio de Janeiro, Brazil) was prepared in acetic acid solution (0.1%, *v/v*) and heated until 70 °C for complete dissolution.

Both solutions were mixed in a 1:1 proportion (in weight), resulting in the sample henceforth referred to as CG11.

MNs of NiFe_2O_4 and CoFe_2O_4 were dispersed into the prepared chitosan–gelatine solution by ultrasonic irradiation for 60 min in the weight ratio polymer: MNs of 1:2, with the samples designated as CG11Ni and CG11Co, respectively. The solutions obtained were cast in acrylic and dried in a refrigerator.

2.2. Characterisation Techniques

The X-ray diffraction (XRD) spectra were obtained, at room temperature, on a Rigaku XDMAX diffractometer (CuK α radiation, $\lambda = 1.54060 \text{ \AA}$ – XDMAX, Rigaku, Tokyo, Japan) at 40 kV and 30 mA.

The microstructure of the samples was observed by scanning electron microscopy (SEM), performed in an Inspect S-50, FEI system (FEI inspect S-50, Hillsboro, OR, USA), on the surface and fracture surface of all the samples, which were previously covered with gold (30 nm) before microscopic observation.

The magnetic measurements were taken using a vibrating sample magnetometer (VSM), from Cryogenics' (London, UK) device. The hysteresis curves were obtained, of 5 and 300 K, with a magnetic field from –10 to 10 T.

For the dielectric characterization, the opposite sides of the samples were covered with silver conducting paste. During the dielectric measurements, samples, with a thickness of about 0.15 mm, were maintained in a helium atmosphere to improve the heat transfer and eliminate the moisture. The impedance spectroscopy measurements were performed in the frequency range of 40 Hz to 1 MHz, as a function of the temperature (120–300 K), using an Agilent 4294A Precision Impedance Analyser (Santa Clara, CA, USA), measuring in the Cp-Rp configuration.

3. Results and Discussion

The X-ray diffraction pattern of the chitosan/gelatin film, CG11, and prepared ferrite composites, CG11Ni and CG11Co, are shown in Figure 1.

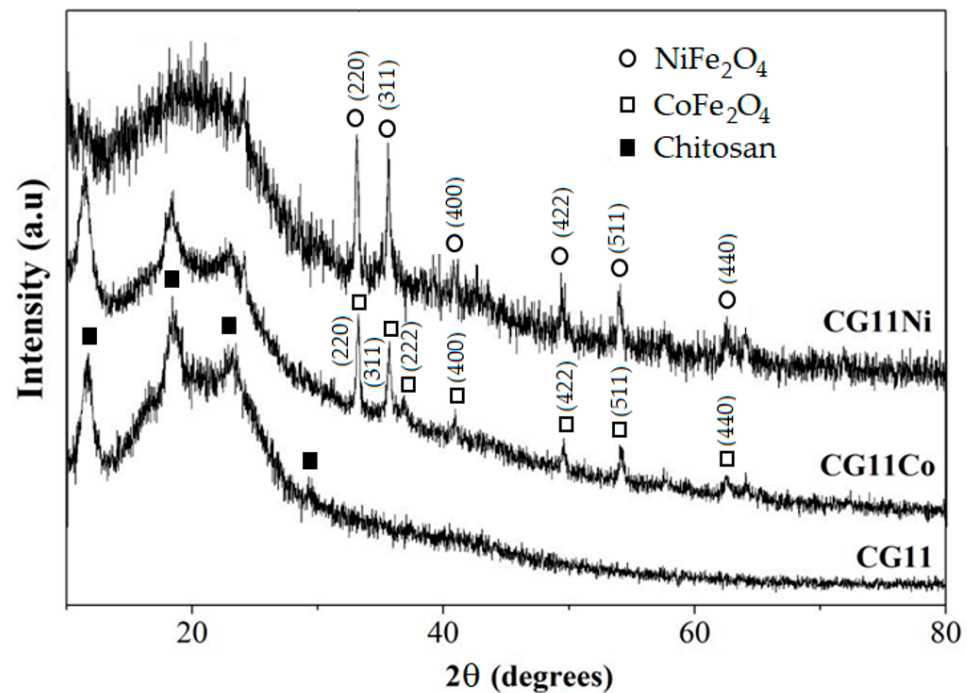


Figure 1. XRD patterns of the studied samples.

For the sample CG11, four distinct peaks, located at $2\theta = 11.9^\circ$, 18.5° , 23.4° and 29.4° , can be observed. These peaks are specific characteristic functional peaks of semi-crystalline chitosan, as shown in the literature [37,38].

Gelatine, which possesses, essentially, a non-crystalline structure, also shows a moderate and very broad peak around 20.0° [39,40]. This fact is well aligned with the presented results, namely due to the amorphous area observed for lower values of 2θ .

The XRD spectrum of the CG11Co samples presents the peaks located at $2\theta = 11.9^\circ$, 18.5° and 23.4° , assigned to chitosan. However, with a slight decrease in their relative intensity. Additionally, six sharp peaks can be well indexed to the inverse cubic spinel structure of CoFe_2O_4 , according to the ICDD 04-016-3954 code [41].

In the CG11Ni sample, none of the peaks ascribed to chitosan are visible. This can be justified by the disruption of the well-crystalline linear structure of chitosan due to interaction with various monomers since amine and hydroxyl groups on the polymeric structure of chitosan interact non-covalently with nanoparticles [42]. However, the five narrow peaks observed can be assigned to NiFe_2O_4 , in agreement with the ICDD 04-014-8286 [43].

These results confirm that the nanoparticles of CoFe_2O_4 and NiFe_2O_4 were successfully synthesized and show that the sample CG11Ni exhibits a loss of crystallinity in the organic phase of the composite, in contrast with the sample CG11Co, which maintains its crystallinity. This shows that the loss of crystallinity is not a result of the preparation process, which might also disrupt the crystalline regions of chitosan and produce a highly amorphous material [44], but due to intrinsic characteristics of the studied nanoparticles.

The crystallite size of Co and Ni ferrites was investigated based on X-ray diffraction line broadening and estimated using Scherrer's equation [36]:

$$d = \frac{B\lambda}{\beta \cos\theta} \quad (1)$$

where d is the average crystallite size of the phase under investigation, B is the Scherrer constant (0.90), λ is the wavelength of the X-ray beam used, β is the full-width half maximum (FWHM) of diffraction and θ is the Bragg's angle. The values obtained were 6.5 nm for CoFe_2O_4 and 7.9 nm for NiFe_2O_4 .

The SEM micrographs of the prepared composites are displayed in Figure 2, where the white dots are the ferrite nanoparticles and the dark background is the chitosan/gelatine polymer. As demonstrated, a good dispersion of the ferrite nanoparticles within the biopolymers network is achieved, particularly in the CG11Co sample. Nevertheless, the formation of aggregates on the surface of both films can be noticed. These agglomerations occur locally due to the magnetic interaction among the cobalt and nickel ferrite nanoparticles [45].

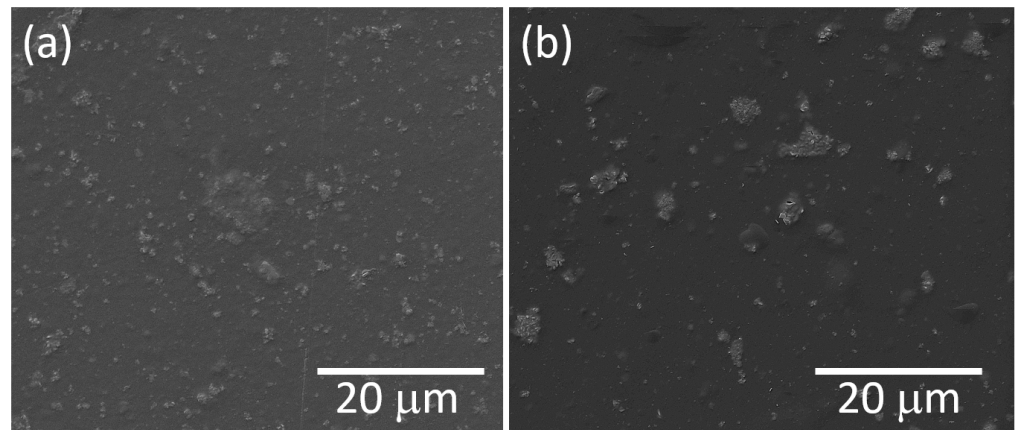


Figure 2. SEM micrographs, taken with a magnification of 5000 \times , of the (a) CG11Co and (b) CG11Ni samples.

It is noteworthy, however, that ferrite nanoparticles are well embedded in the polymer matrix, without visible defects, pores or phase separation unfavourable for device fabrication.

Figure 3 shows the magnetization loops, at 5 K and 300 K of the two composite films, where the variation in the magnetization of the samples CG11Co and CG11Ni was investigated as a function of the magnetic field, in the range of -10 to 10 T [27].

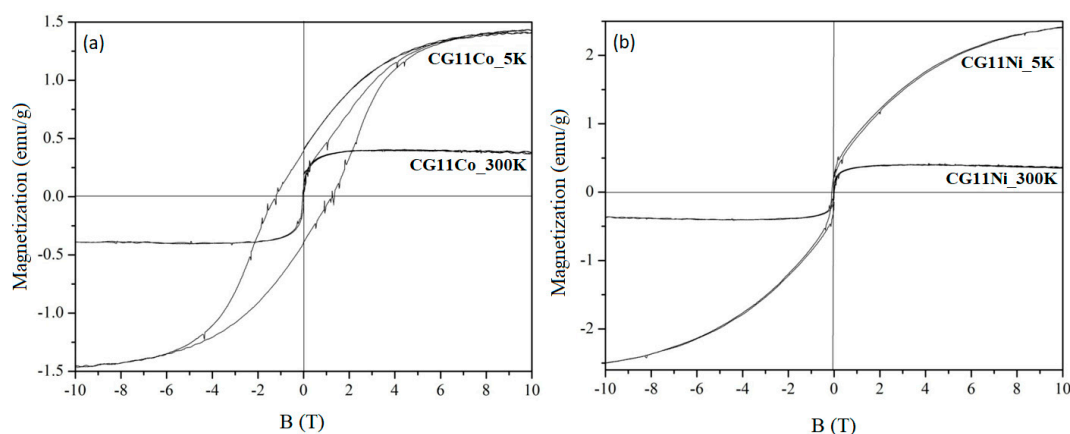


Figure 3. Magnetization hysteresis loop of the (a) CG11Co and (b) CG11Ni samples.

In the case of CG11Co, shown in Figure 3a, the saturation magnetization was found to be 1.43 emu/g at 5 K and 0.36 emu/g at 300 K. This sample shows a coercive force of 1.27 T at 5 K, while at room temperature there is no measurable coercive force.

For the composite CG11Ni, Figure 3b, the saturation magnetization was found to be 2.41 emu/g at 5 K and 0.36 emu/g at 300 K. In this case, a particularly small value of

coercive force is observed, with negligible retentivity, which indicates the ferromagnetic nature of the material in both temperatures.

At room temperature, the saturation magnetization of CoFe_2O_4 nanoparticles, synthesized using the same route, was reported as 29.46 emu/g, with a coercive force of 0.019 T. For the NiFe_2O_4 nanoparticles, the saturation magnetization was 15.2 emu/g, with the coercivity being approximately zero [36].

The formation of an external layer of chitosan/gelatine around the CoFe_2O_4 and NiFe_2O_4 particles provided a composite material with lower magnetization values since both chitosan and gelatine are diamagnetic [46–48]. Also, lower values of the saturation magnetization of the cobalt and nickel ferrites can be due to a disordered surface magnetic layer and noncollinearity of magnetic moments at the octahedral and tetrahedral sites [49].

A similar trend was found by Santos et al. [46], when developing a CoFe_2O_4 /chitosan composite, where the saturation magnetization values were 50.34 and 16.45 emu/g and the coercivity values were 0.032 and 0.031 T for the CoFe_2O_4 particles and CoFe_2O_4 /chitosan, respectively, measured at room temperature.

In the present study, the lower saturation magnetization values of the CG11Co and CG11Ni composites can be due to the gelatine chains that suppress the free rotation of the magnetic moment, as reported by [50] when characterizing composite materials based on gelatine and iron oxide nanoparticles.

The dielectric response of the composites produced, as a function of temperature and frequency, was also studied. The dielectric spectrum of an amorphous polymer generally shows a multiple relaxation behaviour. For each process, a peak in dielectric losses, ϵ'' , is present at a fixed temperature. For a relaxation process, ϵ' and ϵ'' are connected by the Kramers–Kronig relation and contain the same information in principle [51].

Figure 4 shows the variation of ϵ'' as a function of the frequency for the CG11, CG11Co and CG11Ni samples, at temperatures from 120 K to 280 K. A clear increase in the ϵ'' is observed, as a consequence of the cobalt and the nickel ferrites' inclusion on the polymeric matrix, with this increase being more expressive in the sample CG11Ni.

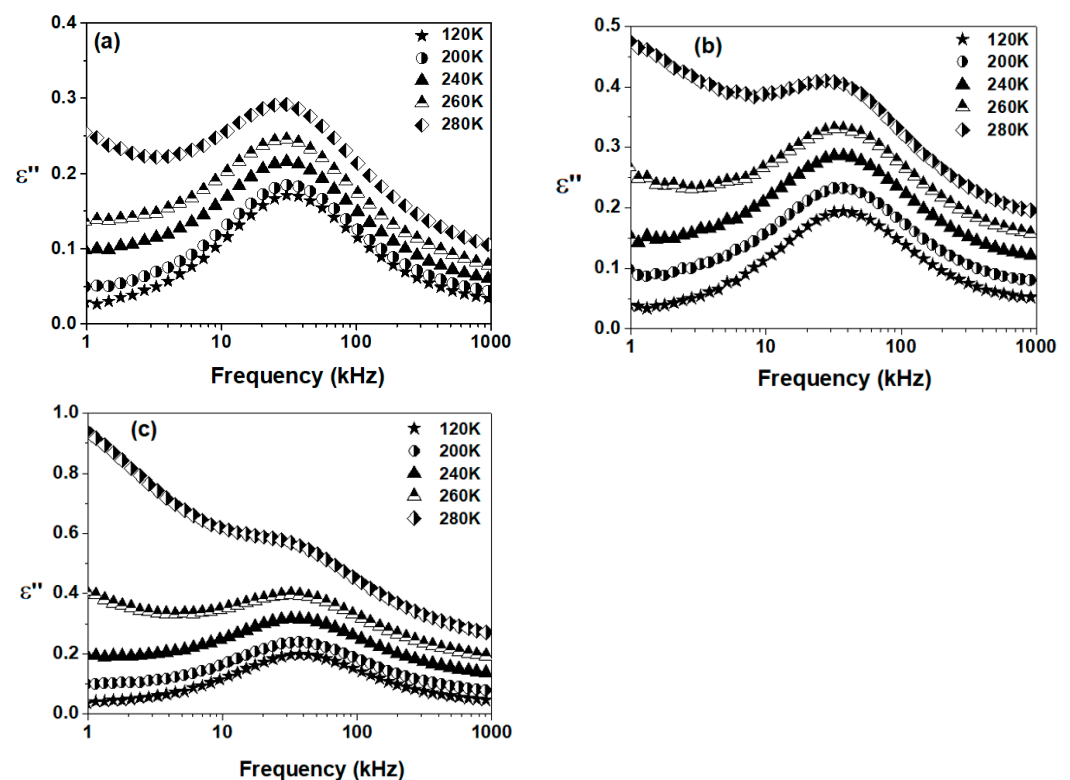


Figure 4. Variation of ϵ'' , as a function of frequency, at temperatures from 120 K to 280 K: (a) CG11; (b) CG11Co; (c) CG11Ni.

An ϵ'' peak can be characterized by its frequency position, f_{\max} , from which the respective relaxation time, $\tau = 1/(2\pi f_{\max})$, can be obtained [52]. As no significant shift in the maximal loss peak occurs with the temperature increase, the relaxation time for the three samples is nearly temperature independent, being displayed in Table 1.

Table 1. Real and imaginary parts of the permittivity, loss tangent, relaxation time and activation energy of the studied samples.

| Sample | ϵ' (280 K, 1 MHz) | ϵ'' (280 K, 1 MHz) | $\tan \delta$ (280 K, 1 MHz) | τ_0 ($\times 10^{-5}$ s) (280 K) | $E_{a(AC)}$ (eV) (1 MHz) |
|--------|----------------------------------|-----------------------------------|------------------------------------|---|--------------------------------|
| CG11 | 3.315 | 0.104 | 0.0314 | 3.462 | 0.248 |
| CG11Co | 3.725 | 0.194 | 0.0521 | 3.128 | 0.250 |
| CG11Ni | 4.456 | 0.267 | 0.0601 | 2.687 | 0.241 |

Table 1 also summarizes the dielectric parameters of the studied samples, obtained at 280 K and 1 MHz. Besides the real and imaginary parts of the permittivity, also known as dielectric constant and dielectric losses, respectively, the loss tangent, given by $\tan \delta = \epsilon''/\epsilon'$ [53], is also presented.

From these results, it is clear that the inclusion of cobalt and nickel ferrites in the chitosan/gelatine film will produce composites with smaller relaxation times, which may be due to interaction at the interface region between the polymer and ferrite particles.

The AC conductivity was calculated using the expression $\sigma_{AC} = \omega \epsilon_0 \epsilon''$ [54] and the Arrhenius expression, given by Equation (2), was applied to estimate the activation energy, where σ_0 is a pre-exponential factor, $E_{a(AC)}$ the activation energy, k_B the Boltzmann constant and T the temperature [55,56]. The activation energy of the three samples is also presented in Table 1.

$$\sigma_{AC} = \sigma_0 \exp\left(\frac{E_{a(AC)}}{k_B T}\right) \quad (2)$$

Figure 5 shows the frequency dependency of the conductivity for the studied samples. The frequency dependency of the conductivity appears almost linear, mainly for temperatures above 240 K. Many works associate such behaviour in collagen and different biological materials to be due to proton polarization and conduction processes [57,58]. It was proposed that these sites are created by newly formed intra- and intermolecular interactions such as hydrogen, hydrogen-bound water, hydrophobic and van der Waals interaction, essential for the stability of the polymeric structure [59]. Such influence on the permittivity seems to be more significant over higher temperature ranges and for the samples with ferrite particles in their composition. The differences in the values of ϵ' and ϵ'' could indicate that the proton transport and the ability of proton accumulation in the interface are lower for CG11 and higher for CG11Ni.

Figure 6 presents the temperature dependency of the real part of the permittivity for the studied samples, at 1 kHz. From these results, a peak of intensity in the ϵ' value around 280 K is visible for the CG11Co and CG11Ni samples and at around 300 K for the CG11 sample.

Differential scanning calorimetry measurements on chitosan [60] show an exothermic peak located approximately from 310 to 398 K and a mass loss associated with this process of 9.2%, which could be due to the evaporation of absorbed water in the inner polymer. In the dielectric measurements, this represents a region of loss increase, as can be seen in Figure 4.

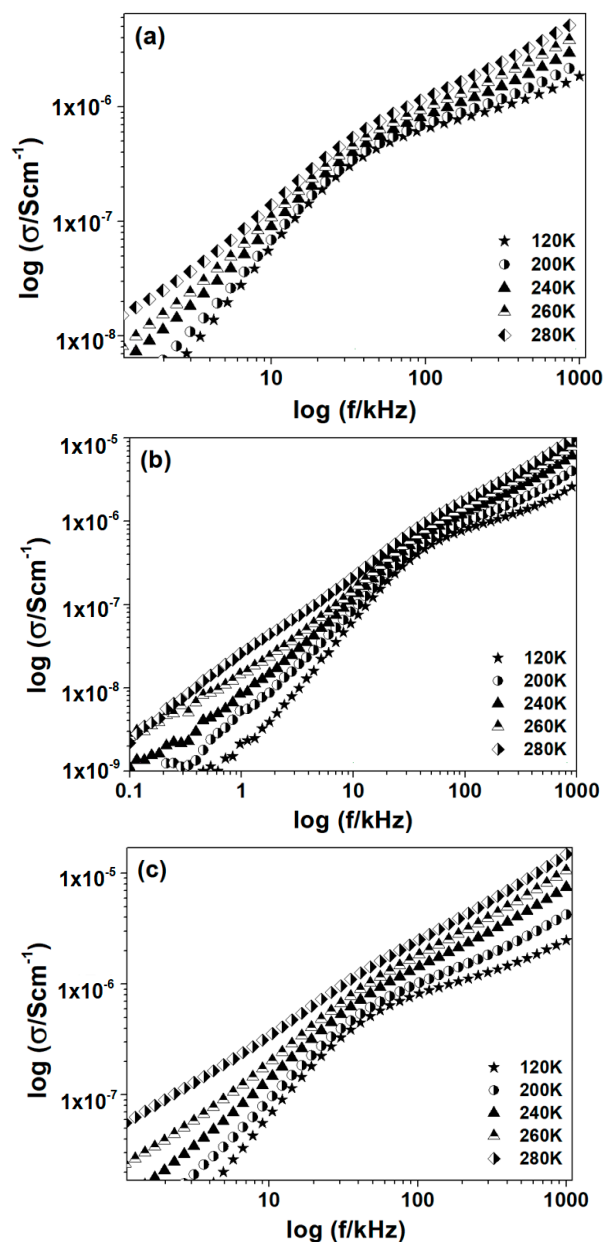


Figure 5. Conductivity, as a function of frequency, at temperatures from 120 K to 280 K: (a) CG11; (b) CG11Co; (c) CG11Ni.

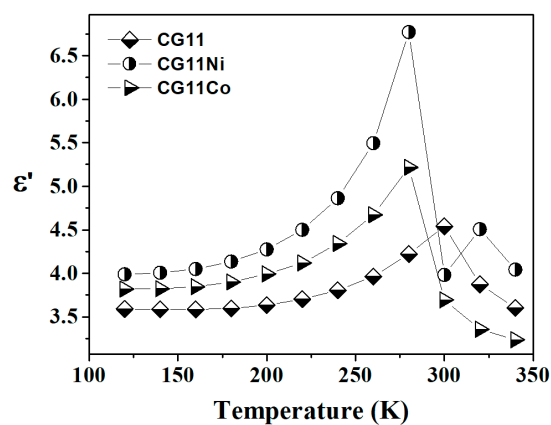


Figure 6. Real part of the dielectric permittivity, as a function of temperature, at 1 KHz.

4. Conclusions

This study investigated the structural, magnetic and dielectric properties of chitosan/gelatine films with embedded ferrite nanoparticles, specifically CoFe_2O_4 and NiFe_2O_4 . The X-ray diffraction patterns confirmed the successful synthesis of the nanoparticles; however, with the CG11Ni exhibiting a loss of crystallinity in the organic phase.

The SEM micrographs demonstrated good dispersion of the ferrite nanoparticles within the biopolymer network, though with some surface aggregates due to magnetic interactions.

The magnetization loops revealed lower saturation magnetization values for both composites compared to bare ferrite nanoparticles, attributed to the chitosan/gelatine coating and, eventually, to disordered surface magnetic layers.

The dielectric response study showed an increase in dielectric losses with the inclusion of ferrites, particularly pronounced in the case of NiFe_2O_4 .

Furthermore, the temperature-dependent real part of permittivity exhibited peaks around 280 K for CG11Co and CG11Ni, and around 300 K for CG11, which can be related to the evaporation of absorbed water in the polymer matrix.

Overall, the findings provide insights into the structural and functional characteristics of the composite materials, validating the ability of ferrite particles and the chitosan/gelatine biopolymer blend to create a naturally occurring composite with magnetic properties, presenting valuable information for potential applications in devices for energy storage, electromagnetic radiation absorbers, magnetic field-activated sensors and, also, for biomedical applications, namely magnetic hyperthermia.

Author Contributions: Conceptualization, J.C.G., S.D.F. and M.P.F.G.; methodology, J.C.G., S.D.F. and M.P.F.G.; software, K.D.A.S. and S.D.; validation, S.D.F. and P.B.A.F.; formal analysis, J.C.G., K.D.A.S. and A.C.H.B.; investigation, S.D.F. and Y.L.N.; A.C.H.B., P.B.A.F. and S.R.G.; resources, M.A.V. and S.R.G.; data curation, J.C.G., P.B.A.F. and S.D.; writing—original draft preparation, J.C.G.; writing—review and editing, S.D.F. and S.D.; visualization, K.D.A.S. and S.D.; supervision, A.S.B.S. and M.A.V.; project administration, A.S.B.S. and M.P.F.G.; funding acquisition, A.S.B.S. and M.P.F.G. All authors have read and agreed to the published version of the manuscript.

Funding: This research was funded by FEDER funds through the COMPETE 2020 Program and National Funds through the FCT—Portuguese Foundation for Science and Technology under the projects LISBOA-01-0247-FEDER-039985/POCI-01-0247-FEDER-039985, LA/P/0037/2020, UIDP/50025/2020 and UIDB/50025/2020 of the Associate Laboratory Institute of Nanostructures, Nanomodelling and Nanofabrication—i3N. S.R. Gavinho acknowledge the FCT—Portuguese Foundation for Science and Technology for the Ph.D. grant (SFRH/BD/148233/2019).

Institutional Review Board Statement: Not applicable.

Informed Consent Statement: Not applicable.

Data Availability Statement: The data presented in this study are available on request from the corresponding author.

Conflicts of Interest: The authors declare no conflicts of interest.

References

1. Ferreira da Silva, M.G.; Valente, M.A. Magnesium Ferrite Nanoparticles Inserted in a Glass Matrix—Microstructure and Magnetic Properties. *Mater. Chem. Phys.* **2012**, *132*, 264–272. [[CrossRef](#)]
2. Indira, T.K.; Lakshmi, P.K. Magnetic Nanoparticles—A Review. *Int. J. Pharma. Sci. Nanotechnol.* **2010**, *3*, 1035–1042. [[CrossRef](#)]
3. Éfendiyev, É.H.; Ali-Zade, R.A.; Zubov, V.P. Synthesis of Polymer Magnetic Microspheres and Study of Their Magnetic Properties. *Crystallogr. Rep.* **2005**, *50*, S168–S172. [[CrossRef](#)]
4. Sharifi, I.; Shokrollahi, H.; Amiri, S. Ferrite-Based Magnetic Nanofluids Used in Hyperthermia Applications. *J. Magn. Magn. Mater.* **2012**, *324*, 903–915. [[CrossRef](#)]
5. Veisheh, O.; Gunn, J.W.; Zhang, M. Design and Fabrication of Magnetic Nanoparticles for Targeted Drug Delivery and Imaging. *Adv. Drug. Deliv. Rev.* **2010**, *62*, 284–304. [[CrossRef](#)] [[PubMed](#)]
6. Medeiros, S.F.; Santos, A.M.; Fessi, H.; Elaissari, A. Stimuli-Responsive Magnetic Particles for Biomedical Applications. *Int. J. Pharm.* **2011**, *403*, 139–161. [[CrossRef](#)] [[PubMed](#)]

7. Wu, H.; Liu, G.; Wang, X.; Zhang, J.; Chen, Y.; Shi, J.; Yang, H.; Hu, H.; Yang, S. Solvothermal Synthesis of Cobalt Ferrite Nanoparticles Loaded on Multiwalled Carbon Nanotubes for Magnetic Resonance Imaging and Drug Delivery. *Acta Biomater.* **2011**, *7*, 3496–3504. [[CrossRef](#)] [[PubMed](#)]
8. Mahmoudi, M.; Sant, S.; Wang, B.; Laurent, S.; Sen, T. Superparamagnetic Iron Oxide Nanoparticles (SPIONs): Development, Surface Modification and Applications in Chemotherapy. *Adv. Drug. Deliv. Rev.* **2011**, *63*, 24–46. [[CrossRef](#)]
9. Srinivasan, S.Y.; Paknikar, K.M.; Bodas, D.; Gajbhiye, V. Applications of cobalt ferrite nanoparticles in biomedical nanotechnology. *Nanomedicine* **2018**, *13*, 1221–1238. [[CrossRef](#)]
10. Yudaev, P.; Butorova, I.; Stepanov, G.; Chistyakov, E. Extraction of Palladium (II) with a Magnetic Sorbent Based on Polyvinyl Alcohol Gel, Metallic Iron, and an Environmentally Friendly Polydentate Phosphazene-Containing Extractant. *Gels* **2022**, *8*, 492. [[CrossRef](#)]
11. Divya, S.; Sivaprakash, P.; Raja, S.; Muthu, S.E.; Eed, E.M.; Arumugam, S.; Oh, T.H. Temperature-Dependent Dielectric and Magnetic Properties of NiFe₂O₄ Nanoparticles. *Appl. Nanosci.* **2023**, *13*, 1327–1336. [[CrossRef](#)]
12. Gasser, A.; Ramadan, W.; Getahun, Y.; Garcia, M.; Karim, M.; El-Gendy, A.A. Feasibility of Superparamagnetic NiFe₂O₄ and GO-NiFe₂O₄ Nanoparticles for Magnetic Hyperthermia. *Mater. Sci. Eng. B* **2023**, *297*, 116721. [[CrossRef](#)]
13. Mullurkara, S.; Fang, Y.; Taddei, K.M.; Wang, G.; Ohodnicki, P. Experimental and Theoretical Investigation of Cation Site Occupation and Magnetic Ordering in CoFe₂O₄. *IEEE Trans. Magn.* **2023**, *59*, 1–5. [[CrossRef](#)]
14. Bilovol, V.; Sikora, M.; Lisníková, S.; Žukrowski, J.; Berent, K.; Gajewska, M. Occupancies of Tetra- and Octahedral Sites in CoFe₂O₄ Nanoparticles: The Effect of the Sintering Temperature. *J. Appl. Phys.* **2023**, *134*, 094304. [[CrossRef](#)]
15. Sivanandan, V.T.; Prasad, A.S. Impact of Green Synthesis on Crystallographic Structure, Optical and Magnetic Properties of Nanocrystalline CoFe₂O₄. *J. Electron. Mater.* **2023**, *52*, 4045–4056. [[CrossRef](#)]
16. Darvishi, M.; Hasani, S.; Mashreghi, A.; Taghi Rezvan, M.; Ziarati, A. Application of the Full Factorial Design to Improving the Properties of CoFe₂O₄ Nanoparticles by Simultaneously Adding Apple Cider Vinegar and Agarose. *Mater. Sci. Eng. B* **2023**, *297*, 116754. [[CrossRef](#)]
17. Chang, P.R.; Yu, J.; Ma, X.; Anderson, D.P. Polysaccharides as Stabilizers for the Synthesis of Magnetic Nanoparticles. *Carbohydr. Polym.* **2011**, *83*, 640–644. [[CrossRef](#)]
18. Philippova, O.; Barabanova, A.; Molchanov, V.; Khokhlov, A. Magnetic Polymer Beads: Recent Trends and Developments in Synthetic Design and Applications. *Eur. Polym. J.* **2011**, *47*, 542–559. [[CrossRef](#)]
19. Rozenberg, B.A.; Tenne, R. Polymer-Assisted Fabrication of Nanoparticles and Nanocomposites. *Prog. Polym. Sci.* **2008**, *33*, 40–112. [[CrossRef](#)]
20. Rezaei, B.; Yari, P.; Sanders, S.M.; Wang, H.; Chugh, V.K.; Liang, S.; Mostufa, S.; Xu, K.; Wang, J.; Gómez-Pastora, J.; et al. Magnetic Nanoparticles: A Review on Synthesis, Characterization, Functionalization, and Biomedical Applications. *Small* **2024**, *20*, e2304848. [[CrossRef](#)]
21. Li, G.; Jiang, Y.; Huang, K.; Ding, P.; Chen, J. Preparation and Properties of Magnetic Fe₃O₄–Chitosan Nanoparticles. *J. Alloys Compd.* **2008**, *466*, 451–456. [[CrossRef](#)]
22. Reddy, N.N.; Varaprasad, K.; Ravindra, S.; Reddy, G.V.S.; Reddy, K.M.S.; Mohan Reddy, K.M.; Raju, K.M. Evaluation of Blood Compatibility and Drug Release Studies of Gelatin Based Magnetic Hydrogel Nanocomposites. *Colloids Surf. A Physicochem. Eng. Asp.* **2011**, *385*, 20–27. [[CrossRef](#)]
23. Chen, J.-P.; Yang, P.-C.; Ma, Y.-H.; Wu, T. Characterization of Chitosan Magnetic Nanoparticles for in Situ Delivery of Tissue Plasminogen Activator. *Carbohydr. Polym.* **2011**, *84*, 364–372. [[CrossRef](#)]
24. Yardımcı, F.S.; Şenel, M.; Baykal, A. Amperometric Hydrogen Peroxide Biosensor Based on Cobalt Ferrite–Chitosan Nanocomposite. *Mater. Sci. Eng. C* **2012**, *32*, 269–275. [[CrossRef](#)]
25. Karthikeyan, P.; Vigneshwaran, S.; Meenakshi, S. Al³⁺ Incorporated Chitosan-Gelatin Hybrid Microspheres and Their Use for Toxic Ions Removal: Assessment of Its Sustainability Metrics. *Environ. Chem. Ecotoxicol.* **2020**, *2*, 97–106. [[CrossRef](#)]
26. Elanchezhian, S.S.D.; Meenakshi, S. Encapsulation of Metal Ions between the Biopolymeric Layer Beads for Tunable Action on Oil Particles Adsorption from Oily Wastewater. *J. Mol. Liq.* **2018**, *255*, 429–438. [[CrossRef](#)]
27. Sheth, Y.; Dharaskar, S.; Khalid, M.; Sonawane, S. An Environment Friendly Approach for Heavy Metal Removal from Industrial Wastewater Using Chitosan Based Biosorbent: A Review. *Sustain. Energy Technol. Assess.* **2021**, *43*, 100951. [[CrossRef](#)]
28. Dash, M.; Chiellini, F.; Ottenbrite, R.M.; Chiellini, E. Chitosan—A Versatile Semi-Synthetic Polymer in Biomedical Applications. *Prog. Polym. Sci.* **2011**, *36*, 981–1014. [[CrossRef](#)]
29. Agrawal, P.; Strijkers, G.J.; Nicolay, K. Chitosan-Based Systems for Molecular Imaging. *Adv. Drug. Deliv. Rev.* **2010**, *62*, 42–58. [[CrossRef](#)]
30. Hritcu, D.; Popa, M.I.; Popa, N.; Badescu, V.; Balan, V. Preparation and Characterization of Magnetic Chitosan Nanospheres. *Turk. J. Chem.* **2009**, *33*, 785–796. [[CrossRef](#)]
31. Yudaev, P.; Semenova, A.; Chistyakov, E. Gel based on modified chitosan for oil spill cleanup. *J. Appl. Polym. Sci.* **2024**, *141*, e54838. [[CrossRef](#)]
32. Mikhailov, O.V. Gelatin as It Is: History and Modernity. *Int. J. Mol. Sci.* **2023**, *24*, 3583. [[CrossRef](#)] [[PubMed](#)]
33. Huss, F.R.M.; Nyman, E.; Bolin, J.S.C.; Kratz, G. Use of Macroporous Gelatine Spheres as a Biodegradable Scaffold for Guided Tissue Regeneration of Healthy Dermis in Humans: An In Vivo Study. *J. Plast. Reconstr. Aesthetic Surg.* **2010**, *63*, 848–857. [[CrossRef](#)] [[PubMed](#)]

34. Gómez-Guillén, M.C.; Giménez, B.; López-Caballero, M.E.; Montero, M.P. Functional and Bioactive Properties of Collagen and Gelatin from Alternative Sources: A Review. *Food Hydrocoll.* **2011**, *25*, 1813–1827. [[CrossRef](#)]
35. Abdeen, Z.I.; Ghoneim, A.I. Improving of the Mg-Co nanoferrites efficiency for crude oil adsorption from aqueous solution by blending them with chitosan hydrogel. *Environ. Sci. Pollut. Res.* **2020**, *27*, 19038–19048. [[CrossRef](#)] [[PubMed](#)]
36. Barreto, A.C.H.; Maia, F.J.N.; Santiago, V.R.; Ribeiro, V.G.P.; Denardin, J.C.; Mele, G.; Carbone, L.; Lomonaco, D.; Mazzetto, S.E.; Fechine, P.B.A. Novel Ferrofluids Coated with a Renewable Material Obtained from Cashew Nut Shell Liquid. *Microfluid. Nanofluidics* **2012**, *12*, 677–686. [[CrossRef](#)]
37. Muley, A.B.; Ladole, M.R.; Suprasanna, P.; Dalvi, S.G. Intensification in Biological Properties of Chitosan after γ -Irradiation. *Int. J. Biol. Macromol.* **2019**, *131*, 435–444. [[CrossRef](#)] [[PubMed](#)]
38. Hartati, H.; Subaer, S.; Hasri, H.; Wibawa, T.; Hasriana, H. Microstructure and Antibacterial Properties of Chitosan-Fe₃O₄-AgNP Nanocomposite. *Nanomaterials* **2022**, *12*, 3652. [[CrossRef](#)] [[PubMed](#)]
39. He, B.; Wang, X.; Xue, H. The Performance of Chitosan/Gelatin Composite Microspheres in the Wash-off Procedure of Reactive Dyeing. *Color. Technol.* **2016**, *132*, 353–360. [[CrossRef](#)]
40. Peng, J.; Wang, X.; Lou, T. Preparation of Chitosan/Gelatin Composite Foam with Ternary Solvents of Dioxane/Acetic Acid/Water and Its Water Absorption Capacity. *Polym. Bull.* **2020**, *77*, 5227–5244. [[CrossRef](#)]
41. Bartolomé, E.; Cayado, P.; Solano, E.; Ricart, S.; Gázquez, J.; Mundet, B.; Coll, M.; Puig, T.; Obradors, X.; Valvidares, M.; et al. Magnetic Stability against Calcining of Microwave-Synthesized CoFe₂O₄ Nanoparticles. *New J. Chem.* **2016**, *40*, 6890–6898. [[CrossRef](#)]
42. Shokri, S.; Shariatifar, N.; Molaee-Aghaee, E.; Khaniki, G.J.; Sadighara, P.; Faramarzi, M.A.; Mohammadi, M.; Rezagholizade-Shirvan, A. Synthesis and characterization of a novel magnetic chitosan–nickel ferrite nanocomposite for antibacterial and antioxidant properties. *Sci. Rep.* **2023**, *13*, 15777. [[CrossRef](#)] [[PubMed](#)]
43. Tuzi, S.; Stiller, K.; Thuvander, M. Oxidation of Alloy X-750 with Low Iron Content in Simulated BWR Environment. *J. Nucl. Eng.* **2023**, *4*, 711–722. [[CrossRef](#)]
44. Jia, Z.; Yang, C.; Zhao, F.; Chao, X.; Li, Y.; Xing, H. One-Step Reinforcement and Deacidification of Paper Documents: Application of Lewis Base—Chitosan Nanoparticle Coatings and Analytical Characterization. *Coatings* **2020**, *10*, 1226. [[CrossRef](#)]
45. Liu, X.; Liu, S.; Han, M.-G.; Zhao, L.; Deng, H.; Li, J.; Zhu, Y.; Krusin-Elbaum, L.; O’Brien, S. Magnetoelectricity in CoFe₂O₄ Nanocrystal-P(VDF-HFP) Thin Films. *Nanoscale Res. Lett.* **2013**, *8*, 374. [[CrossRef](#)] [[PubMed](#)]
46. dos Santos, J.M.N.; Pereira, C.R.; Pinto, L.A.A.; Frantz, T.; Lima, É.C.; Foletto, E.L.; Dotto, G.L. Synthesis of a Novel CoFe₂O₄/Chitosan Magnetic Composite for Fast Adsorption of Indigotine Blue Dye. *Carbohydr. Polym.* **2019**, *217*, 6–14. [[CrossRef](#)] [[PubMed](#)]
47. Lemine, O.M.; Alanazi, A.; Albert, E.L.; Hjiri, M.; M’hamed, M.O.; Alrub, S.A.; Alkaoud, A.; Abdullah, C.A.C. γ -Fe₂O₃/Gd₂O₃-chitosan magnetic nanocomposite for hyperthermia application: Structural, magnetic, heating efficiency and cytotoxicity studies. *Appl. Phys. A* **2020**, *126*, 471. [[CrossRef](#)]
48. Deuffhard, M.; Eberbeck, D.; Hietschold, P.; Wilharm, N.; Mühlberger, M.; Friedrich, R.P.; Alexiou, C.; Mayr, S.G. Magnetically responsive composites: Electron beam assisted magnetic nanoparticle arrest in gelatin hydrogels for bioactuation. *Phys. Chem. Chem. Phys.* **2019**, *21*, 14654–14662. [[CrossRef](#)] [[PubMed](#)]
49. Gurgel, A.L.; Martinelli, A.E.; de Aquino Conceição, O.L.; Xavier, M.M.; Morales Torres, M.A.; de Araújo Melo, D.M. Microwave-Assisted Hydrothermal Synthesis and Magnetic Properties of Nanostructured Cobalt Ferrite. *J. Alloys Compd.* **2019**, *799*, 36–42. [[CrossRef](#)]
50. Drobot, M.; Vlad, S.; Gradinaru, L.M.; Bargan, A.; Radu, I.; Butnaru, M.; Rîmbu, C.M.; Ciobanu, R.C.; Aflori, M. Composite materials based on gelatin and iron oxide nanoparticles for MRI accuracy. *Materials* **2022**, *15*, 3479. [[CrossRef](#)]
51. Bordewijk, P. *Theory of Electric Polarization*; Elsevier: Amsterdam, The Netherlands, 1978.
52. Devesa, S.; da Silva, P.S.P.; Graça, M.P.; Costa, L.C.; Paixão, J.A. Impedance Spectroscopy Studies of ErNbO₄ Synthesised by the Sol–Gel Method. *J. Sol-Gel Sci. Technol.* **2020**, *96*, 143–152. [[CrossRef](#)]
53. Devesa, S.; Gonçalves, F.; Graça, M. Influence of the Preparation Method on the Structural, Morphological and Dielectric Properties of FeNbO₄ Ceramics. *Materials* **2023**, *16*, 3202. [[CrossRef](#)]
54. Devesa, S.; Graça, M.P.; Henry, F.; Costa, L.C. Dielectric Properties of FeNbO₄ Ceramics Prepared by the Sol-Gel Method. *Solid State Sci.* **2016**, *61*, 44–50. [[CrossRef](#)]
55. Lima, M.M.R.A.; Monteiro, R.C.C.; Graça, M.P.F.; Ferreira da Silva, M.G. Structural, Electrical and Thermal Properties of Borosilicate Glass–Alumina Composites. *J. Alloys Compd.* **2012**, *538*, 66–72. [[CrossRef](#)]
56. Graça, M.P.F.; Prezas, P.R.; Costa, M.M.; Valente, M.A. Structural and Dielectric Characterization of LiNbO₃ Nano-Size Powders Obtained by Pechini Method. *J. Sol-Gel Sci. Technol.* **2012**, *64*, 78–85. [[CrossRef](#)]
57. Samouillan, V.; Lamure, A.; Lacabanne, C. Dielectric Relaxations of Collagen and Elastin in the Dehydrated State. *Chem. Phys.* **2000**, *255*, 259–271. [[CrossRef](#)]
58. Gulino, M.; Bellia, P.; Falciglia, F.; Musumeci, F.; Pappalardo, A.; Scordino, A.; Triglia, A. Role of Water Content in Dielectric Properties and Delayed Luminescence of Bovine Achilles’ Tendon. *FEBS Lett.* **2005**, *579*, 6101–6104. [[CrossRef](#)]

59. Marzec, E.; Warchoł, W. Dielectric Properties of a Protein–Water System in Selected Animal Tissues. *Bioelectrochemistry* **2005**, *65*, 89–94. [[CrossRef](#)]
60. López, F.A.; Mercé, A.L.R.; Alguacil, F.J.; López-Delgado, A. A Kinetic Study on the Thermal Behaviour of Chitosan. *J. Therm. Anal. Calorim.* **2008**, *91*, 633–639. [[CrossRef](#)]

Disclaimer/Publisher’s Note: The statements, opinions and data contained in all publications are solely those of the individual author(s) and contributor(s) and not of MDPI and/or the editor(s). MDPI and/or the editor(s) disclaim responsibility for any injury to people or property resulting from any ideas, methods, instructions or products referred to in the content.